

http://pubs.acs.org/journal/aesccq Article

Atmospheric Processing of Anthropogenic Combustion Particles: Effects of Acid Media and Solar Flux on the Iron Mobility from Fly Ash

Deborah Kim, Yao Xiao, Renee Karchere-Sun, Emily Richmond, Heather M. Ricker, Angelina Leonardi, and Juan G. Navea*



Cite This: ACS Earth Space Chem. 2020, 4, 750-761



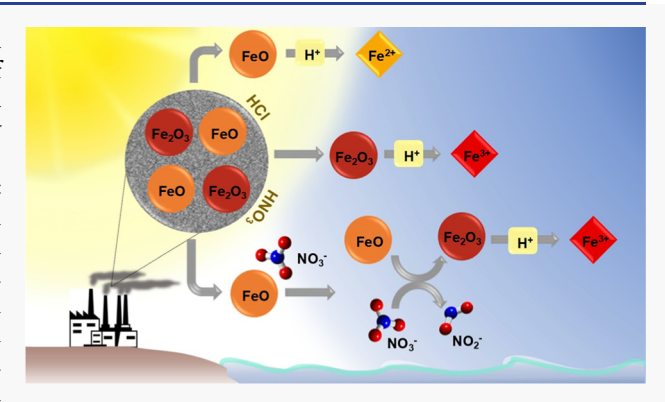
ACCESS

Metrics & More

Article Recommendations

s Supporting Information

ABSTRACT: Atmospheric combustion particles, such as fly ash emitted from coal-fired power plants, are a potential source of atmospheric iron, with significant implications in climate and global biogeochemical cycles. While the iron content and speciation of fly ash depend closely on the source region and combustion process, few studies have been carried out comparing the atmospheric processing of fly ash produced from coal-fired power plants in different regions. In this study, we present an investigation of iron dissolution in acidic aqueous solutions: HNO₃ and HCl at pH 1 and pH 2 under daytime and nighttime conditions for three fly ash samples from three different sources: United States (USFA), Central Europe (EUFA), and India fly ash (INFA). Iron mobility and speciation depend on the source region and the combustion



efficiency that generates fly ash. In HCl suspensions, proton-promoted mechanisms lead to larger fractions of aqueous-phase iron leached from fly ash particles, with poorly combusted samples providing significant fractions of Fe²⁺. In HNO₃ suspensions, a surface-mediated redox reaction suppresses the mobility of Fe²⁺, leading to the formation of nitrites. In the presence of solar radiation, previously unrecognized pathways of atmospheric processing enhance the formation Fe²⁺ and nitrous acid from combustion particles. The information provided herein could be significant to increase our understanding of the effects of combustion particles in the atmospheric chemical balance regarding iron and nitrites.

KEYWORDS: aerosol, particulate matter, metal transport, aerosol dissolution, bioavailable iron

■ INTRODUCTION

Despite its relative abundance on Earth's crust, iron is a limiting micronutrient essential for the metabolic functioning of marine organisms. 1-3 For instance, dissolved and bioavailable iron is known to stimulate phytoplankton growth, affecting the global carbon cycle by modulating CO2 sequestration and influencing global climate.^{4,5} In isolated regions of the ocean, one of the more likely sources of soluble bioavailable iron is atmospheric particulate matter deposition. 6-8 However, the alkaline pH of seawater on the surface of the ocean (pH \approx 8) does not dissolve iron-containing minerals from atmospheric particle depositions. 9,10 The amount of aqueous phase iron in high-nutrient low chlorophyll suggests that iron is mobilized in the more acidic atmospheric environment, before and during aerosol deposition. 11 In fact, atmospheric processing has been shown to dissolve ironcontaining mineral dust and urban aerosol particles effectively via proton-promoted mechanisms and chelation processes. 10,12-16 Recently, atmospheric mobilization of anthropogenic combustion iron has been found to be a significant

climate forcer with an estimated radiative forcing of 21 mW m⁻¹ globally.¹⁷ Nevertheless, significant uncertainties remain regarding the effects of iron speciation in the rates and yield of iron mobility from anthropogenic combustion particles.

Recent studies suggest that atmospheric processing of fly ash (FA), which are combustion particles emitted from coal-fired power plants, is an important source of soluble iron and an important parameter in the Earth's climate system. ^{18–23} For example, in China, increasing annual emissions of FA are currently estimated to be in the range of 31 Tg, and in Europe, FA emission is estimated to be 90 Tg per year. ^{24–27} Given the particle size and morphology of FA, it can be transported from urban areas to remote regions of the oceans and can undergo

Received: February 27, 2020
Revised: April 22, 2020
Accepted: April 23, 2020
Published: April 23, 2020





Table 1. Iron Content and Surface Area in FA Samples: United States Fly Ash (USFA), Northeast India Fly Ash (INFA), European Fly Ash (EUFA), and Mullite^a

sample	total iron $(mg g^{-1})$	surface area (m² g ⁻¹)	average size (most probable size) (μ m)	observation summary
USFA	38 ± 2	1.8 ± 0.1	$1.59 \pm 0.05 \ (0.89 \pm 0.08)$	fully combusted. Main component: mullite.
INFA	25 ± 3	2.07 ± 0.04	$2.07 \pm 0.05 \ (1.21 \pm 0.06)$	fully combusted. Main component: mullite
EUFA	9.4 ± 0.8	2.8 ± 0.1	$4.6 \pm 0.2^{A} (2.2 \pm 0.3)^{A}$	partially combusted, containing reduced elements. Main components: mullite and feldspars. Larger content of copper species.
mullite	n.o.	3.3 ± 0.2	n.o.	standard "iron-free" aluminosilicate $(3Al_2O_3 \cdot 2SiO_2)$

^an.o.: none observed; A: calculated from spherical particles only.

atmospheric processing, impacting the atmospheric balance. 28,29 Similar to mineral dust, FA interacts with the highly acidic deliquescent layer formed around its particles by the uptake of water and acidic atmospheric gases (pH $\approx 0-3$). For mineral dust, the rate of iron dissolution depends not only on the pH but also on the mineralogy of the particles, the solar flux, and the identity of the acid. 13,31,32 One important atmospheric acid is nitric acid (HNO₃), primarily generated from nitrogen oxide atmospheric reactions. As an oxidizing acid, HNO₃ can impact the speciation of iron, while daytime conditions have shown to drive surface reactions of HNO3 on semiconductors and chromophores present in these atmospheric aerosols.³³ In fact, recent studies in our research group suggest that HNO3 heterogeneous photochemistry on metal oxides, common components of combustion particles, can lead to nitrous acid formation and the renoxification of the atmosphere.^{34–36} However, little is known about the rate and yields of these reactions in the acidic deliquescent layer around FA particles during atmospheric transport.

Recent global model simulations suggest that iron mobility from anthropogenic combustion particles in the atmosphere play a key role in present-day ocean biogeochemical cycles and atmospheric aerosols.¹⁷ However, large uncertainties suggest the need for laboratory experiments in order to better understand the processes that control the solubility of iron, including the rate of solubility and yields. While sample composition, solar flux, and the identity of the acid can influence the iron mobility from FA, additional parameters, such as the efficiency of the combustion process and the source region, need to be included in current atmospheric models. This work investigates the effect of the FA source (iron content and speciation because of the combustion process) on the mobility of iron in the atmosphere, including the effect of combustion efficiency, pH, and solar flux, in a protonpromoted dissolution using HCl and in the presence of HNO₃. We carried out dissolution experiments simulating the acidic deliquescent layer of FA particles, evaluating the role of iron speciation in the formation of the nitrite ion in atmospheric water at both daytime and nighttime. Our results highlight the impact of combustion efficiency in iron dissolution along with its potential role in the nitrogen atmospheric cycle.

■ EXPERIMENTAL SECTION

Source Materials. FA samples, classified as FA C, were collected at the electrostatic precipitators of single power plants located in different regions: United States of America (USFA) from the Midwest region, Indian fly ash (INFA) from Northeastern India, and European fly ash (EUFA) from a commercially available standard of FA (BCR-176R) obtained from the European Commission. The significant difference in

geographical location of the emitting power plants secures not only a source region comparison but also different coal sources. The characterization of these samples has been reported and discussed in recent publications by our research group. ^{18,28} Briefly, elemental analysis carried out with X-ray fluorescence (XRF) and atomic absorption spectroscopy (AAS) indicate that the main trace metal component of all FA samples is iron, as summarized in Table 1 and Table S1 in the Supporting Information section. ¹⁸ In Figure 1, X-ray diffraction (XRD)

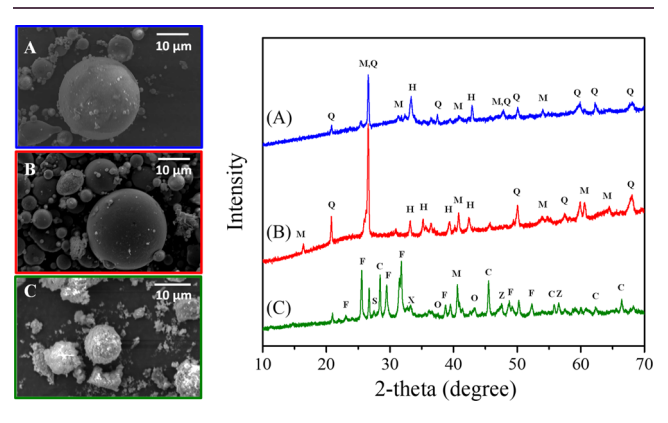


Figure 1. Left: Representative micrographs of FA samples. (A) United States (USFA); (B) Northeast India (INFA); (C) European fly ash (EUFA). Right: XRD characterization of FA samples. (A) USFA; (B) INFA; (C) EUFA. XRD legend: Q-quartz; M-mullite; H-hematite/magnetite; F-feldspar; C-calcite; Z-zinc oxide; S-copper(I) sulfide; O-copper(I) oxide; X-copper(II) oxide.

patterns of the samples and standards show structural and compositional differences between the samples. The main component of all FA samples is mullite (3Al₂O₃·2SiO₂), formed from the combustion of clay components of coal, with EUFA showing more diffraction patterns because of a richer composition with the presence of calcium feldspars.²⁸ There are also important diffraction peaks indicating the presence of quartz (SiO₂), with traces of hematite (Fe₂O₃) and magnetite (Fe₃O₄).^{37,38} The XRD spectra in Figure 1 also show a broadening feature between 15 and 35°, especially noticeable in INFA, characteristic of an amorphous phase of silica in the glassy FA particles. As discussed in a previous publication from our group, XRD and Fourier transform infrared (FTIR) also show evidence of calcite in EUFA, further suggesting incomplete combustion of this sample. The incomplete combustion of EUFA was further confirmed using scanning electron microscopy (SEM) as shown in Figure 1. EUFA micrographs show amorphous rock-like particles, indicating incomplete combustion in contrast to the micrograph of USFA and INFA samples showing predominantly spherical particles formed during a highly efficient combustion process. Infrared

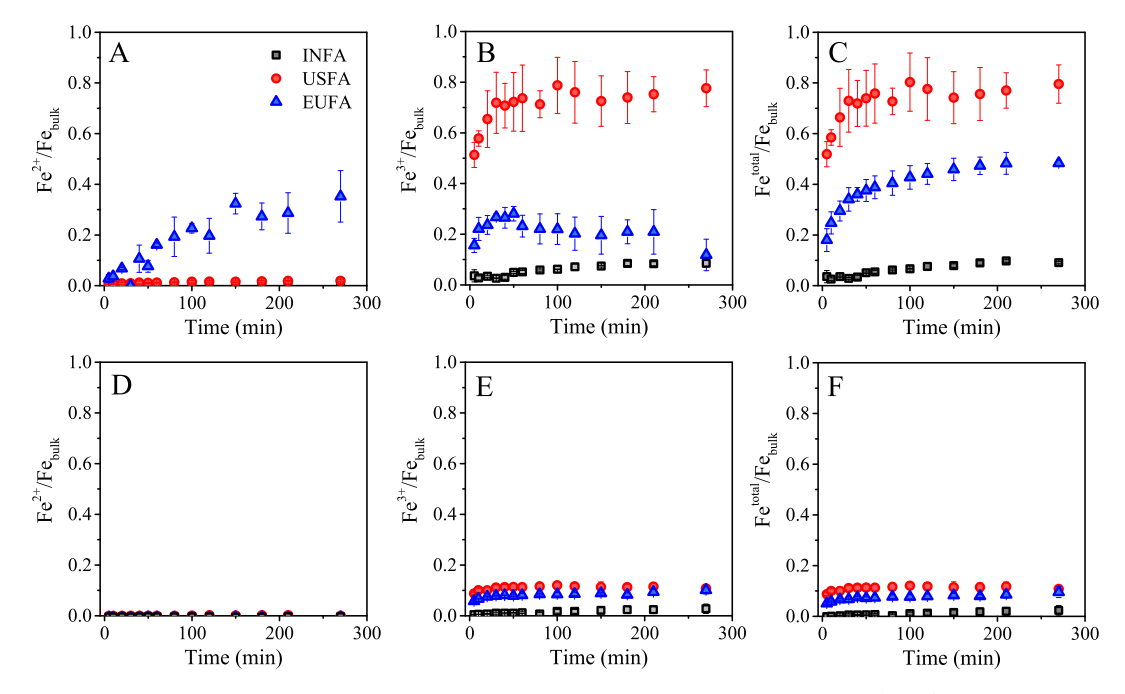


Figure 2. Fraction of Fe species dissolved from FA at pH = 1.0 in the absence of sunlight. Top graphs (A-C) represent iron leaching in HCl suspensions; bottom graphs (D-F) represent iron leaching in HNO₃. Graphs A and D represent the fraction of Fe²⁺ dissolved; graphs B and E represent the fraction of Fe³⁺ dissolved; graphs C and F represents total iron in solution $(Fe^{total} = Fe^{2+} + Fe^{3+})$. Graphs showing data up to 50 h of suspension in the Supporting Information.

spectroscopy of EUFA (Figure S1, Supporting Information) shows features centered at 1411 and 1628 cm⁻¹, assigned to the bending mode of carbonates and a stretching mode of bicarbonates. No carbonate or bicarbonate bands were detected in USFA and INFA, suggesting a significantly different level of combustion between EUFA and the rest of the samples.

Iron oxide species in FA have been shown to bind with species such as SO_4^{2-} and CO_3^{2-} , which is particularly important for EUFA, $^{39-41}$ as carbonates are already present in the bulk of the sample as a result of an incomplete combustion. Thus, as CO_3^{2-} dissolve in the acidic deliquescent layer, EUFA particles can lose physical integrity and breakup into smaller fragments, leading to higher iron dissolution. Small traces of carbonates can be detected in INFA (feature at 46° in Figure 1); no clear evidence of CO_3^{2-} was found in USFA.

All reagents used for sample characterization and dissolution experiments were of analytical grade. Further trace elemental analysis using XRF spectroscopy can be found in the Supporting Information (Figure S1 and Table S1). The specific surface areas (S_{BET}) , measured using an 11-point Brunauer-Emmet-Teller (BET) surface analyzer (Quantacrome e400), show that European fly ash has the highest S_{BET} of the three samples examined because of defects and porosity present in non- or partially-combusted components such as feldspars. Average particle sizes and most probable sizes, summarized in Table 1, are obtained from a minimum of 350 particle counts from SEM micrographs, as reported by Borgatta et al.¹⁸ Particle sizes are comparable to FA particle sizes from several field studies, with an average particle size <2.5 μ m but with distributions as large as 40 μ m. 42-45 Finally, a commercially available mullite standard (Alfa Aesar) was used as a control in suspension experiments to represent "ironfree FA."

Suspension Experiments. The acidic deliquescence layer mobilizing iron from atmospheric particles has pHs as low as 1 or 2, and its effect over the dissolution of combustion particles can depend on the acidic anion's reducing or oxidizing agent.¹⁴ To study these effects, dissolution of iron species was performed on FA suspensions of 1 g L⁻¹ in constantly stirred solutions acidified with hydrochloric acid or nitric acid to a controlled pH set to 1.0 \pm 0.1 or 2.0 \pm 0.1. The acidic processing of combustion particles was simulated in a 300 mL custom-built jacketed beaker with an airtight quartz window top for oxygen-free and daytime experiments at 298 K.¹⁸ Aliquots were periodically taken from the reaction vessel using disposable syringes and filtered through 0.2 μ m pore size polytetrafluorothylene filters for iron and nitrite analysis. Control experiments were performed using mullite, the main aluminosilicate component of FA, confirming that no iron originated from the reaction vessel or other external sources. Although an important fraction of iron dissolution takes place within the first 300 min, all suspension experiments were carried out for a minimum of 50 h to ensure equilibrium and simulate atmospheric transport periods.

Because Fe^{3+} shows low solubility above pH 3.6, it was determined that the conditions mentioned above most accurately simulated cloud processing of tropospheric aerosol particles that could drive iron mobility. ^{29,30} Under our experimental conditions, Fe^{3+} above 60 ppm begins to precipitate as $Fe(OH)_3$ above pH 2.4.³¹ Thus, an upper pH limit of 2.0 \pm 0.1 allows for the measurement of Fe^{3+} in solution without hydrolysis loss of iron. ²⁵ Even though the rate of ferrous iron oxidation is slow, its dependency on pH can lead to oxygenation of Fe^{2+} , particularly as the pH increases. ³² In order to prevent oxidation of Fe^{2+} once leached from FA, all dissolution experiments were carried out under a constant nitrogen purge to prevent oxidation by dissolved oxygen. Prior to the suspension experiment, the acidic solution was purged

by bubbling nitrogen for 15 min to obtain a deoxygenated solution; the dissolution experiment was then carried out with a continuous flow of 5 sccm of nitrogen above the solution surface to maintain an oxygen-free atmosphere throughout the experiment. This low oxygen environment allowed for a better quantification of both Fe³⁺ and Fe²⁺ leached from FA samples during the suspension experiments, in particular allowed for the calculation of iron speciation as it relates to initial rates of dissolution.^{31,47} In addition, to control the variations in ionic strength in the suspension solution as the dissolution of FA particles takes place, all acidic solutions were adjusted to 1.0 M NaCl for HCl suspensions and 1.0 M NaNO₃ for HNO₃ suspensions.

Iron and nitrite quantification started at a t = 0 min, defined as the moment of FA loading into the acid solution. After t = 0min, the suspension aliquots were colorimetrically analyzed for dissolved iron and nitrite ion content.³³ As reported in a previous work, dissolved iron speciation was quantified using 1,10-phenanthroline, which selectively forms an orange complex with Fe2+ with an absorbance band at 510 nm. Total dissolved iron was quantified in the same samples by adding hydroxylamine to reduce all Fe3+ to Fe2+ prior to phenanthroline complexation. The absorbance measured via the colorimetric method was converted into concentrations using aqueous standards prepared from anhydrous ferrous chloride (Sigma-Aldrich). Nitrite ion formation was quantified using the Griess reagent (Promega), which forms a pink complex in the presence of nitrite, with an absorbance band of 563 nm. Similarly, standards of the nitrite ion (Promega) were used to determine the concentration of the nitrite ion. colorimetric measurements were performed in triplicate using a Lambda 35 PerkinElmer UV/vis spectrophotometer.

All suspension experiments were performed under nighttime and daytime conditions. For the latter, a solar simulator with a 150 W xenon lamp (Oriel Corp.) was placed above the reaction chamber providing solar radiation at a constant power of 136.2 mW/cm² at the top of the reaction chamber, which is comparable to one solar constant. To determine the photon flux in the reaction batch, which accounts for penetration depth of the light source, the intensity of light in the solution was determined using potassium ferrioxalate ($K_3Fe(C_2O_4)_3$ · $3H_2O$), a well-known chemical actinometer. Under our experimental conditions, the light flux in the batch reactor was in average (6.4 \pm 0.2) \times 10⁻⁶ E min⁻¹.

■ RESULTS AND DISCUSSION

Nighttime Iron Mobility: Role of pH and Acidic Anion. Iron mobility and speciation were investigated in the absence of light. Figure 2 shows the time progression of total dissolved Fe, Fe2+, and Fe3+ for the three different ashes suspended in a reducing acid, HCl, and an oxidizing acid, HNO3, solutions at pH 1 (a pH 2 figure is available in the Supporting Information, Figure S3). All three ashes show an increase in the fraction of dissolved iron with respect to their initial iron content as reported in Table 1. The two main mechanisms controlling the iron dissolution from FA are proton-promoted, observed in HCl, and a combination of proton and ligand-promoted in an HNO₃ suspension. ^{22,23,30,34,47} These dissolution mechanisms depend on surface $H^{\scriptscriptstyle +}$ and $OH^{\scriptscriptstyle -}$ functional groups reacting with $H^{\scriptscriptstyle +}$ and/ or NO₃-, weakening the surface structures and ultimately mobilizing iron into the aqueous phase. 48-50 For all combustion particles examined here, the highest fraction of total iron leached was observed from USFA, with roughly 80 and 10% of iron partitioning to the aqueous phase in HCl and HNO₃ pH 1 solutions, respectively. Conversely, the lowest fraction of iron leached was observed from INFA, reaching total iron fraction in aqueous phase around 10 and 3% of its bulk iron content in HCl and HNO₃, respectively, over 300 min of suspension. While aqueous phase iron from USFA and EUFA reached a maximum at 300 min, a continuous iron leach was observed over 50 h of INFA suspension, reaching nearly 40% of its iron content into aqueous phase in HCl (see Supporting Information, Figure S2).

Although all samples examined here mostly consist of an aluminosilicate matrix, the varying combustion process and mineralogical characteristics resulted in chemical and structural differences that control iron solubility and speciation.²⁸ Initially, any surface iron species in immediate contact with the acidic media dissolves quickly as the initial layer of the particle dissolves, resulting in a fast dissolution pathway.¹⁸ In general, FA particles are glassy spheroids formed after efficient combustion followed by fast cooling.^{51,52} Chemical bonds in these well-combusted aluminosilicate glass matrices are weaker and more susceptible to attacks by protons than feldspars found in mineral dust or partially combusted ashes.²⁰ Thus, when FA particles dissolve, they break up into smaller fragments, allowing for better contact between the acidic media and iron, which leads to a second, slower pathway of iron leaching into the solution phase. These two pathways were observed for well-combusted samples (USFA and, to a lesser extent, INFA) and feldspar-rich partially combusted samples (EUFA). However, the rate and fractions of dissolved iron are strikingly different in each sample, as discussed below.

As anticipated from the thorough combustion of both USFA and INFA, the iron leached from these samples is almost all Fe³+, with Fe²+ fractions under 3% in 1.0 N HCl suspensions. For EUFA, the incomplete combustion leads to a larger fraction of Fe²+ mobility in the HCl suspension, with 60 \pm 8% of the total dissolved iron being Fe²+ after 300 min of suspension. This higher aqueous phase concentration of Fe²+ is produced from the dissolution of magnetite, a common component in partially combusted coal as shown in equations below 18,49

$$\frac{1}{2} Fe_2 O_3(s) + 3H^+(aq) \rightarrow Fe^{3+}(aq) + \frac{3}{2} H_2 O(l) \tag{1}$$

$$FeO(s) + 2H^{+}(aq) \rightarrow Fe^{2+}(aq) + H_2O(l)$$
 (2)

$$Fe_3O_4(s) + 8H^+(aq)$$

$$\rightarrow Fe^{2+}(aq) + 2Fe^{3+}(aq) + 4H_2O(l)$$
(3)

Reactions 1–3 indicate that the proton-promoted mechanism also consumes protons, which, along with other mineral components such as carbonates and bicarbonates, can result in pH changes. Thus, for the duration of the suspension experiments, the pH was kept constant by adding microliters of concentrated HCl into the suspension, with no statistically significant dilution factor in the iron concentrations. As shown in Figure 2 (and Supporting Information), soluble iron from USFA and EUFA exhibit the two pathways at pH 1 and 2: an initial rapid release of iron, followed by a slower iron leach. The fast iron dissolution pathway, which takes place at a time scale faster than our experimental resolution (<5 min), suggests the presence of surface iron species in direct contact

Table 2. Initial Rate of the Fast (v_f) and Slow (v_s) Dissolution Pathways of Iron Species Leached from FA Suspensions in $HCl^{a,b}$

		$\nu_{\rm f}~(\times 10^{13}~{ m molec.~cm^{-3}~s^{-1}})$			$v_{\rm s}~(\times 10^{13}~{\rm molec.~cm}^{-3}~{\rm s}^{-1})$		
pН	sample	Fe ²⁺	Fe ³⁺	total Fe	Fe ²⁺	Fe ³⁺	total Fe
1	USFA	0.78 ± 0.10	70 ± 7	71 ± 7	0.2 ± 0.1	4.9 ± 0.8	5.1 ± 0.8
		0.8 ± 0.5	51 ± 3	52 ± 3	0.26 ± 0.09	5.0 ± 0.9	5.1 ± 0.9
	INFA	n.o	1.2 ± 0.2	1.1 ± 0.2	0.04 ± 0.03	0.17 ± 0.09	0.17 ± 0.07
		n.o	n.o	n.o	n.o	0.22 ± 0.06	0.22 ± 0.02
	EUFA	1.0 ± 0.5	5.6 ± 0.6	6 ± 2	0.55 ± 0.10	0.6 ± 0.2	1.1 ± 0.4
		1.5 ± 0.8	12 ± 2	10 ± 2	n.o	0.9 ± 0.4	0.8 ± 0.1
2	USFA	0.18 ± 0.08	7.6 ± 0.9	7.7 ± 0.9	0.07 ± 0.06	5.9 ± 0.8	6.0 ± 0.8
		n.o	12 ± 6	11 ± 5	n.o	7.0 ± 0.5	7.1 ± 0.7
	INFA	n.o	0.3 ± 0.4	0.3 ± 0.4	n.o	0.19 ± 0.01	0.204 ± 0.003
		0.27 ± 0.10	n.o	n.o	0.06 ± 0.06	n.o	0.15 ± 0.09
	EUFA	n.o	0.5 ± 0.6	0.5 ± 0.6	n.o	0.2 ± 0.1	0.33 ± 0.02
		2.1 ± 0.5	3 ± 2	3.8 ± 0.5	0.4 ± 0.2	0.8 ± 0.2	1.2 ± 0.3

^aDark experiments are in the shaded rows and irradiated experiments are in the nonshaded rows. The errors are the standard deviation over, at least, triplicate experiments. ^bn.o.: not observed.

with the acidic solution. In contrast, iron mobility from INFA did not show a significant rapid iron dissolution pathway, likely due to a lower iron leach from the sample and less surface iron content.¹⁸ While the fast dissolution pathway was also observed in pH 2 solutions, at higher pH, the generation of soluble iron species dropped and the rate of the dissolution decreased, in agreement with mechanisms driven by the concentration of protons as described in reactions 1 and 2. In previous studies in our laboratory, we reported that FA dissolution was strongly dependent on pH, with higher iron dissolution taking place at lower pHs. 18 Consistent with these observations, at pH 1.0, iron dissolution takes place at faster rates and produces higher yields than that of pH 2.0 suspensions. Given that proton-promoted dissolution is the main mechanism driving iron mobility from FA samples in an HCl suspension, the increase in the fraction of iron dissolved with the decrease in pH is consistent with reactions 1 and 2.

For HCl suspensions, the initial rapid leach of total iron $(Fe^{3+} + Fe^{2+})$, v_{t} , was estimated to be the concentration at 5 min of suspension: at pH 1 suspensions in HCl, (0.8 \pm 0.1) \times 10^{13} and $(1.0 \pm 0.5) \times 10^{13}$ molec. cm⁻³ s⁻¹ for USFA and EUFA, respectively. At pH 2, the rapid iron dissolution from USFA decreased to 25% of its value in the more acidic media, while for EUFA, the value of v_f decreased to roughly half the value at pH 1. The slow pathways, v_s , were estimated as the initial rate starting at 5 min. It has been suggested that the specific surface area of the samples play an important role in iron solubility. 53,54 While the specific surface area could play a role in the fast pathway of iron leach, for combusted particles, surface area does not correlate with iron mobility. Our results suggest that iron solubility and speciation from FA particles are chemically driven, depending mostly on the source region and combustion process. The differences in the dissolved iron fractions also imply that iron mobility from combustion particles is inherently dependent on the combustion process and the concomitant mineralogy of the particles, with the only predictable correlation being the larger relative fraction of Fe²⁺ in solution for poorly combusted particles. This lack in correlation is comparable to iron mobility processes from mineral dust samples.¹⁴ Conversely, differences in iron speciation depend on combustion efficiency. The iron dissolution rates are summarized in Tables 2 and 3.

Table 3. Initial Rate of the Fast (v_f) and Slow (v_s) Dissolution Pathways of Iron Leached from FA Suspensions in HNO₃ a,b

pН	sample	$\nu_{\rm f}~(\times 10^{13}~{\rm molec.~cm^{-3}~s^{-1}})$	$\nu_{\rm s}~(\times 10^{13}~{\rm molec.~cm^{-3}~s^{-1}})$
1	USFA	11.6 ± 0.7	0.6 ± 0.1
		37 ± 2	n.o
	INFA	n.o	0.050 ± 0.003
		n.o	0.048 ± 0.009
	EUFA	1.7 ± 0.2	0.18 ± 0.01
		1.4 ± 0.2	0.15 ± 0.03
2	USFA	5.5 ± 0.5	1.2 ± 0.2
		4 ± 2	0.7 ± 0.2
	INFA	n.o	0.031 ± 0.004
		0.2 ± 0.2	0.04 ± 0.03
	EUFA	0.3 ± 0.1	0.17 ± 0.08
		0.5 ± 0.1	0.13 ± 0.05

"Only Fe³⁺ is observed to leach into solution in the presence of HNO₃. Dark experiments are in the shaded rows, and irradiated experiments are in the nonshaded rows. The errors are the standard deviation over, at least, triplicate experiments. ^bn.o.: not observed.

In EUFA, the concentration of Fe²⁺ continuously increases throughout the dissolution time. Conversely, a slight decline in the concentration of Fe³⁺ is observed in EUFA suspensions after the first hour of suspension, suggesting a reduction of Fe³⁺ in solution. This reduction process is more noticeable in daytime experiments, as it will be discussed in the next section. Overall, the reduction of dissolved Fe³⁺ suggests the presence of a reducing agent in EUFA that is not present in the nearlycompletely oxidized components of USFA and INFA. Furthermore, the larger amount of spectral features in the EUFA XRD spectrum shown in Figure 1 indicates a much more complex mineralogy, including compounds such as ZnO and copper species such as CuO, Cu2O, and Cu2S. These species are commonly present in FA samples but in different proportions depending on its source region and the combustion process. 55,56 The presence of copper(I), as for iron(II), in EUFA is mostly the result of an incomplete combustion process characteristic of this sample. Furthermore, copper AAS analysis of all FA samples showed that EUFA contains (720 \pm 10) μ g g⁻¹ of Cu, about 5 times more than USFA and 36 times more than INFA. The presence of Cu(I)

or other nonoxidized trace elements or components can lead to the reduction of a fraction of the dissolved Fe³⁺

$$Cu^{+}(aq) + Fe^{3+}(aq) \rightarrow Cu^{2+}(aq) + Fe^{2+}(aq)$$
 (4)

Given that the free energy change for the redox reaction above is estimated to be -59.62 kJ mol⁻¹, the Fe³⁺ reduction pathway is thermodynamically favored in EUFA acidic media suspension. While other trace reducing agents can be present, the higher fraction of Cu in EUFA, along with the standard reduction potential of Cu⁺, seems to be the dominating reducing agent, with a correlation between solution-phase copper (Figure S5) and the drop in concentration of Fe³⁺. Reaction 4 has a fast electron transfer between Cu⁺ and Fe³⁺ in solution, with most leachable copper dissolving at pH < 5.57-59Effects on pH over the Cu/Fe redox coupling can become significant in the presence of peroxides and peroxyradicals, which are negligible under the anaerobic suspensions described here. Overall, incomplete combustion leading to reduced species within the FA particle can potentially open a redox pathway for the formation of Fe²⁺. However, since the reducing agent components of EUFA are limiting, in the absence of a continuous source of Cu⁺, reaction 4 can only contribute to a small extent in the formation of Fe2+ and the decrease of solution-phase Fe³⁺.

In the presence of HNO₃, surface iron leaches from FA via the H⁺ effect and by nitrate ions chelating Fe in a ligandpromoted mechanism. In the HNO3 suspension, two key differences are observed: first, less soluble iron at lower rates is generated; second, the formation of Fe2+ is suppressed, even in the partially combusted EUFA sample, which contains a relatively higher fraction of Fe²⁺. As indicated above, under oxygen-free conditions, the iron solubility mechanism in HNO3 is not only through proton-promoted but also proceeds via chelation of iron with nitrate ions. In contrast with the monodentate complex between chloride ions and iron in the HCl suspension, nitrate ions on the deliquescent layer of FA can bind with surface iron to form monodentate, bidentate, and bridging complexes. While this complex formation can promote the leaching of iron, the lower concentrations of total iron in solution indicate that the ligand-promoted mechanism is less effective in leaching particle iron than proton-promoted mechanisms. This observation is in good agreement with similar experiments conducted in mineral dust suspensions. 12,14,23 Similar to the dissolution process in HCl for USFA and EUFA, in HNO3, most of the iron dissolution takes place in the first rapid step, with more than 60% of the iron leached over the first 300 min of suspension dissolving in under 5 min. As mentioned above, the fast pathway, which controls the larger fraction of iron mobility in USFA and EUFA, decreases in HNO₃ suspensions. For INFA, this fast pathway is not observed and total iron leaches slowly into the solution phase. At pH 1.0, the ratio of fast dissolution rates of Fe³⁺, $\frac{[\nu_f \text{ in HCl}]}{[\nu_f \text{ in HNO}_3]}$, shows that in the HNO₃ suspension, the rate of iron mobility from FA decreases by a factor of six for USFA and by a factor of nearly four for EUFA. This initial rate ratio between HCl and HNO₃ suspensions is not as significant at pH 2, where the initial rates for HCl suspensions is around 1.5 times larger than those in HNO3 for both USFA and EUFA. This pH dependency suggests that, while there is a ligandpromoted mechanism involving the binding modes between NO₃ and iron, there is a parallel proton-promoted mechanism as well. In the case of INFA, the initial rate ratio of the slow

iron dissolution pathway, $\frac{[\nu_s \text{ in HCl}]}{[\nu_s \text{ in HNO}_3]}$, increases at a higher pH due to the fact that the slow pathway becomes the only pathway for iron mobility in INFA at pH 2.0, with no observed fast pathway for iron dissolution.

In the presence of nitrates, the absence of aqueous-phase Fe^{2+} is attributed to the reduction of nitrates, with Fe^{2+} acting as the reducing agent, as indicated by half-reactions 5 and 6

$$2Fe^{2+}(aq) \rightarrow 2Fe^{3+}(aq) + 2e^{-}$$
 (5)

$$2e^{-} + 2H^{+} + NO_{3}^{-}(aq) \rightarrow NO_{2}^{-}(aq) + H_{2}O$$
 (6)

With the overall reaction

$$2H^{+} + NO_{3}^{-}(aq) + 2Fe^{2+}(aq)$$

 $\rightarrow 2Fe^{3+}(aq) + NO_{2}^{-}(aq) + H_{2}O$ (7)

Figure 3A shows the relative increase of nitrite concentration with respect of time. For the European sample of fly ash (EUFA), the relatively larger fraction of reducing agent Fe²⁺, as observed in the iron leached from the HCl suspension (Figure 2A), leads to a higher concentration of NO₂⁻. Conversely, the sample from Northeast India (INFA) has the lowest availability of Fe²⁺ both per iron content in FA and per surface area, leading to the lowest fraction of nitrites from the three samples examined. Control experiments carried out with suspensions of iron-free mullite, the main aluminosilicate in FA, showed no detectable NO₂⁻, indicating that nitrites are formed primarily by iron in FA.²⁸ Figure 3A also shows that, as the pH increased, the formation rate and yield of nitrite decreased, much more significantly for EUFA, the sample with a significant fraction of Fe²⁺. While the decrease in nitrite

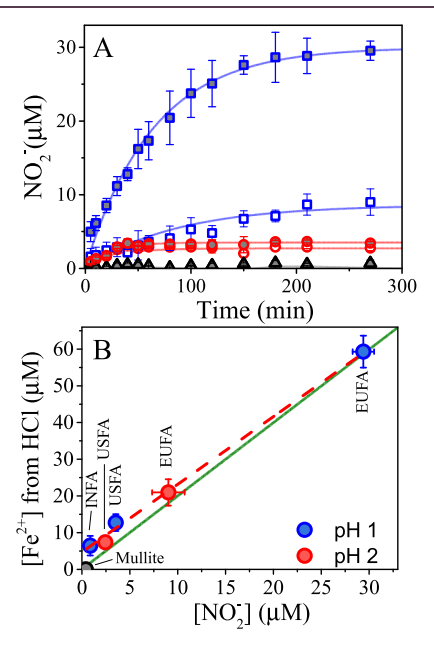


Figure 3. (A) Nitrite formation at pH 1 (gray-filled symbols) and at pH 2 (clear symbols) conditions. Blue squares (■) represent EUFA, red circles (●) represent USFA, and black triangles (▲) represent INFA. (B) Stoichiometric relation available Fe^{2+} as determined in HCl suspensions and NO_2^- from HNO₃ suspensions. The ratio Fe^{2+} : NO_2^- was determined by the slope (dashed red line) of 1.85 \pm 0.05. Green line corresponds to the 2:1 stoichiometric relation from reaction 3.

formation in USFA and INFA is less significant, the overall drop in nitrite formation is in agreement with reaction 7, which requires acidic media for the reduction of nitrates with Fe²⁺ as the limiting reagent.

Standard reduction potentials for half-reaction 4 ($E_o = 0.771$ V) and half-reaction 5 ($E_0 = 0.94$ V) indicate that the reduction of nitrate by Fe²⁺ in acidic solution is thermodynamically favorable, with a change in Gibbs free energy (ΔG) of -16.3 kJ mol $^{-1.61}$ However, even assuming that all the iron found in solution is the result of the oxidation of Fe2+ by NO_3^- , there is 5 times more NO_2^- present in solution than is predicted by eq 7. Thus, the total amount of iron in solution cannot account for the complete reduction of nitrates in the HNO₃ suspension. A kinetic interpretation from Fu et al. suggests that nitrate reduction by iron-containing minerals is a surface-mediated reaction, implying that nondissolved Fe²⁺ can still reduce surface NO₃^{-.12} In fact, there is a stoichiometric correlation between the amount of Fe2+ mobilized from FA suspensions in HCl and the concentration of NO₂⁻ measured in HNO₃ suspensions. Figure 3B shows that the experimentally determined stoichiometric relation of 1.85:1 for Fe²⁺:NO₂ (red dashed line) is in good agreement with the theoretically determined 2:1 relation from reaction 7 (green line), suggesting that nitrite loss is not significant at the concentrations formed during reaction. This observation suggests that the reduction of nitrate by ferrous oxide involves all the iron content in FA that would be otherwise mobilized during a proton-promoted dissolution in an HCl suspension, consistent with a surface-mediated mechanism. However, the slight underestimation of NO₂⁻ for USFA and INFA suggests that not all the iron dissolved in the HCl suspension became available to interact and reduce nitrate ions in the HNO3 solution, likely due to the higher efficiency of the protonpromoted dissolution that drives the iron solubility in HCl. This argument is in agreement with multiple studies indicating that Fe²⁺ contained in the surface of minerals is a stronger reducing agent than aqueous-phase Fe²⁺. In addition, nitrate formed during reaction 6 can be lost via surfacemediated effects and by partitioning into the atmosphere above the reaction vessel, a potential pathway for daytime HONO formation. 34,35,46 There are two mechanisms involving leachable iron from FA (determined by the HCl suspensions) as the reducing agent of nitrate: first, surface iron(II) oxide and Fe²⁺ present within the aluminosilicate of FA (\equiv Fe²⁺(s)) acts as a reducing agent of nitrate. Second, Fe²⁺ leached into the solution phase is readsorbed as Fe3+ onto the suspended FA after an initial acid-promoted dissolution. 12 Either mechanism is consistent with the low concentrations of iron in HNO3 solutions compared to that in HCl. The absence of any trace Fe²⁺ at the shortest time scales is also evidence that the reduction of nitrate by Fe²⁺ is a surface-mediated process. Scheme 1 summarizes the nighttime mechanisms leading to iron mobility for both HCl and HNO3 suspensions.

Role of Solar Radiation on Iron Mobility. The iron dissolution and speciation from each FA sample were also investigated under simulated solar radiation, with the same variables used in nighttime experiments. Figure 4 mirrors Figure 2, showing a time progression for all three samples at pH 1 up to 300 min (a pH 2 figure is available in the Supporting Information, Figures S2 and S3). As observed during nighttime experiments, all three FA samples show an increase in the fraction of dissolved iron with respect of time. The presence of simulated sunlight has different effects

Scheme 1. Iron Mobility from FA at Nighttime, with $\equiv \text{Fe}^{2+}(s)$ Representing the Fe^{2+} Content within the Aluminosilicate of FA; NO_2^- (a) Represents Surface Adsorbed Nitrite

$$= Fe^{2^{+}}_{(s)} \xrightarrow{FeO_{(s)}} FeO_{(s)} \xrightarrow{H^{+}} Fe^{2^{+}}_{(aq)} \xrightarrow{Cu^{+}_{(aq)}} Cu^{+}_{(aq)}$$

$$= Fe^{2^{+}}_{(s)}, FeO_{(s)} \xrightarrow{Fe_{2}O_{3(s)}} Fe^{3^{+}}_{(aq)} \xrightarrow{Fe^{3^{+}}_{(aq)}} Fe^{3^{+}}_{(aq)} \xrightarrow{Fe^{3^{+}}_{(aq)}} Fe^{3^{+}}_{(aq)} + NO_{2^{-}_{(aq)}}$$

depending on the degree of combustion of the sample and the acid anion. In the HCl batch reaction, the dissolved iron fraction and speciation at daytime and nighttime from INFA is statistically similar at all times of suspension. Over the first 300 min, only EUFA shows a significant enhancement in yield of total dissolved iron (Figure 4C) of around 40% in the presence of light compared to the dark reaction over the same time scale. For USFA, a small but measurable enhancement of Fe²⁺ was observed in the rate of iron dissolution by its slow pathway at pH 1.0 (Table 2). In addition, a photoreduction of Fe³⁺ into Fe2+ is observed in USFA and EUFA samples. For USFA, photoreduction over 50 h of irradiation increases the concentration of aqueous Fe^{2+} from (1.3 ± 0.2) ppm in dark conditions to (3.0 ± 0.2) ppm (see Supporting Information, Figure S2), in agreement with similar studies on mineral dust and oil and bituminous FA samples at the same pH. 12,21-23 However, when compared to studies conducted with mineral dust and synthetic particles, the photoreduction enhancement in USFA samples is significantly lower mostly because of the lower concentration of α -Fe₂O₃ in the FA samples, which is <2%, at least an order of magnitude lower than the ironcontaining samples in these studies. 12,31,32

At pH 2.0, the lower dissolution of iron makes the photoreduction effect statistically not observable. A photoreduction mechanism has been reported to be more effective in the presence of surface hydroxyl groups that reduce the Fe³⁺ ions on the surface of the particles, which then detach and yields Fe²⁺ via a proton-promoted dissolution. ¹² Therefore, the effect of solar radiation depends highly on the mineralogy of the FA particle. The role of mineralogy in the photoreduction of Fe³⁺ ions is more evident in the dissolution of iron under simulated sunlight for EUFA at pH 2.0, where the fraction of aqueous Fe²⁺ doubles compared to the dark reaction over 50 h of suspension (Figure S3). In EUFA suspensions, the mobility of total iron increases from (6.5 ± 0.8) ppm under dark conditions to (8.5 ± 0.4) ppm under daytime conditions after 50 h of suspension. The initial rate of iron dissolution from EUFA also increases significantly, mostly for the fast pathway, indicating that most of the leachable iron partitions to the solution phase in less than 5 min under our experimental conditions. As shown in Figure 4, most of the initial iron dissolution from EUFA is Fe³⁺, which undergoes photoreduction to form Fe2+. This redox effect is similar to that of EUFA suspensions under dark conditions: the concentration of Fe³⁺ starts to decline after 60 min of suspension while aqueous Fe2+ increases. However, it is clearly enhanced in the presence of sunlight. This photoreduction can be because of two

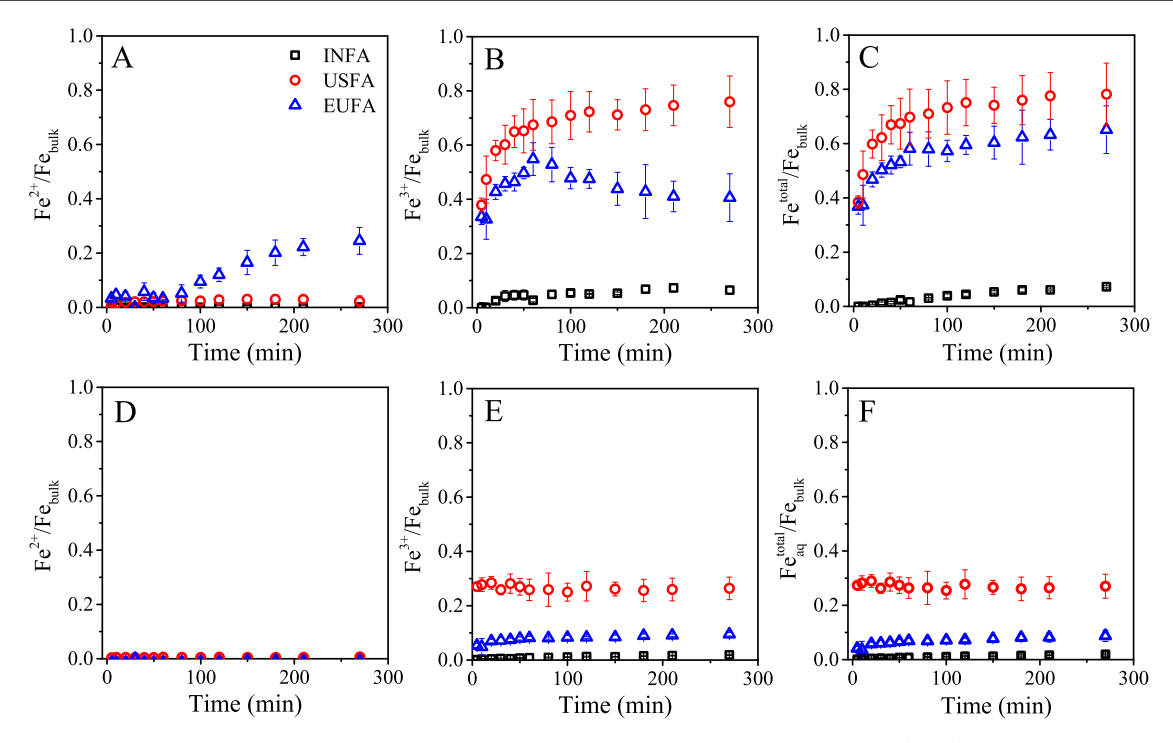


Figure 4. Fraction of Fe species dissolved from FA at pH = 1.0 in the presence of sunlight. Top graphs (A–C) represent iron leaching in HCl suspensions; bottom graphs (D–F) represent iron leaching in HNO₃. Graphs A and D represent the fraction of Fe²⁺ dissolved; graphs B and E represent the fraction of Fe³⁺ dissolved; graphs C and F represents total iron in solution (Fe^{total} = Fe²⁺ + Fe³⁺). Graphs showing data up to 50 h of suspension in the Supporting Information.

competing pathways: a solution-phase photoreduction of Fe³⁺ and a surface-mediated reaction.

The solution-phase photoreduction in HCl depends on complexation and pH. At low pHs and in the presence of Clions, Fe3+ forms predominantly two complexes: [Fe- $(OH_2)_5Cl]^{2+}$ and $[Fe(OH_2)_4Cl_2]^+$. These aqueous species are photoactive within the solar spectral region, reacting with light to release chlorine radicals and the Fe2+ species $[Fe(OH_2)_6]^{2+}$, ultimately increasing the fraction of Fe^{2+} in solution. ^{12,32,65} In the presence of HNO₃, this mechanism is suppressed, as Fe³⁺ does not readily forms an aqueous complex with nitrates. A surface-mediated photoreduction reaction can be triggered by semiconductor metal oxides present in FA particles, such as hematite, α -Fe₂O₃, and, at a lower concentration, TiO_2 . The semiconductor band gap of α -Fe₂O₃ is about 2.2 eV, or 564 nm, while TiO₂ band gap is around 3.07 eV, corresponding to 404 nm. Both energy gaps are smaller than the cutoff for solar radiation in the troposphere and our solar simulator under experimental conditions (290 nm). $^{33-35,66}$ Thus, photoirradiation of the batch reactor can induce redox reactions initiated by electrons in the conduction band (e_{cb}^{-}) and the concomitant hole in the valence band (h_{vb}^{+}) , as described in reactions 8 and 9

$$\alpha - \text{Fe}_2 \text{O}_3 + h\nu \ (\lambda < 564 \text{ nm}) \rightarrow \text{h}_{vb}^{+} + \text{e}_{cb}^{-}$$
 (8)

$$h_{vb}^{+} + e_{cb}^{-} \rightarrow recombination$$
 (9)

While semiconductor effects are expected to be relatively low, given that these components are in trace amounts in the FA particles, their effects can have important implications. The highly mobile e_{cb}^- can trigger reduction reactions and has been reported to photoreduce Fe^{3+} , particularly effectively in the absence of oxygen²³

$$Fe^{3+}(aq) + e_{cb}^{-} \rightarrow Fe^{2+}(aq)$$
 (10)

In the case of INFA, the sample with the lowest concentration of α -Fe₂O₃, no measurable enhancement of solution Fe2+ was observed in the presence of simulated sunlight. Conversely, EUFA shows the largest photoreduction effect. We hypothesize that this relatively large solution-phase photoreduction enhancement in EUFA suspensions is because of the Cu-Fe redox coupling characteristic of the Cucontaining EUFA sample described in the previous section. The clear enhancement of the redox coupling observed in the drop of Fe³⁺ at around 60 min of reaction can be the result of two effects. First, a higher dissolution of iron can result in a higher loss of the particle's physical integrity, leading to higher dissolution of copper, which is the limiting reagent in reaction 4. Second, similar to observations involving the presence of HO_2 in acidic media proposed by Mao et al., 57,58 aqueous Cu^{2+} produced in reaction 4 can be reduced by the conduction band electron in a process analogous to reaction 10

$$Cu^{2+}(aq) + e_{cb}^{-} \rightarrow Cu^{+}(aq)$$
 (11)

where Cu⁺ is regenerated and available to reduced Fe³⁺ via reaction 4, which can be the dominant reduction pathway because of a relatively fast electron transfer of $1.3-3\times 10^7~M^{-1}~s^{-1}.^{57,58}$ The holes (h_{vb}^{+}) generated in reaction 8, while highly oxidizing, have a lower mobility than the conduction band electrons (e_{cb}^{-}) . Thus, h_{vb}^{+} tends to react with water near the surface of the particle leading to the formation of hydroxyl radicals

$$H_2O(a) + h_{vb}^+ \to OH(a) + H^+(a)$$
 (12)

where the small fraction of OH radicals will likely react quickly with the surface of the particle, increasing the OH density on the surface. ^{28,35} The trace concentrations of semiconductor

metal oxide in FA prevent OH radicals generated in reaction 12 to oxidize significantly the low concentration of aqueous phase iron.

Similar to nighttime observations, in HNO₃ suspensions under light irradiation, no Fe²⁺ was detected because of the surface-mediated reduction of NO₃⁻ to NO₂⁻, described in reaction 7. The photoinduced enhancement of iron dissolution is apparently inhibited by the HNO₃ media for INFA and EUFA, which is in good agreement with Fe-containing mineral dust experiments. 12,23,64 However, USFA does show an enhanced iron mobility at daytime compared to nighttime in the same time scale: the total iron in solution doubles under simulated solar radiation and the slow pathway is effectively suppressed, with all the iron dissolved under 5 min of suspension, as shown in Figure 3E,F. We interpret this photolytic effect as an enhancement because of the higher presence of semiconductor α -Fe₂O₃, which can get excited via reaction 8 and break up the aluminosilicate structure into smaller fragments, effectively increasing the iron solubility. 12-14 These clear differences in iron mobility further suggest that the source region and combustion process that lead to combustion particles might play a significant role in their atmospheric processing and iron mobility. In addition, Figures 2 and 4 suggest that photolytic dissolution of iron from FA depends on the acid anion, in agreement with recent work from Hettiarachchi and Rubasinghege, which suggests that the acid anion plays a key role in photoreductive processes that lead to bioavailable Fe²⁺ from atmospheric aerosol.³²

During photolysis experiments, an additional pathway for nitrite loss opens via photolytic decomposition 67-69

$$NO_2^-(aq) + H_2O(l) \xrightarrow{h\nu} NO(aq) + OH(aq) + OH^-(aq)$$
(13)

Surface-mediated oxidation can also be induced via the formation of NO2, which can partition to gas-phase during the time scale of the experiment.³⁵ The OH radicals formed by reactions 12 and 13 have been shown to enhance the reduction of surface Fe³⁺ to Fe²⁺, especially in particles containing large amounts of α -Fe₂O₃. ^{32,47,70-72} However, as shown in Figure 4, no significant enhancement of Fe2+ was observed during the photolysis experiments in HNO₃ because of the relatively low concentrations of α -Fe₂O₃ in FA compared to that in mineral dust. In addition, the absence of dissolved oxygen and the relatively low concentrations of NO₂⁻(aq) formed during the reaction time scale lead to relatively low concentrations of the OH radical, making its effect on iron mobility negligible compared to the acidic media and solar flux. Under our experimental conditions, the rate of photolytic decomposition of aqueous NO₂ follows a pseudo-first-order kinetics rate law, as shown by the green dashed line in Figure 5, with a rate constant of $(1.68 \pm 0.06) \times 10^{-4} \,\mathrm{s}^{-1}$ and a lifetime in the batch reactor of (60 ± 2) min. Thus, NO_2^- formed via the surfacemediated reaction 7 will be consumed by a consecutive photolytic reaction that should decrease the yield of nitrite. This photolytic loss of NO₂⁻ is observed in EUFA suspension experiments, the partially combusted sample, where the pseudo-steady-state concentration of NO₂⁻(aq) drops from 30 μ M under dark conditions to 17 μ M under simulated solar radiation. This 47% loss in NO₂⁻ formation is in good agreement with reaction 13. However, Figure 5 shows the opposite effect for USFA and INFA samples, the two samples that are fully oxidized, where the concentration of NO₂

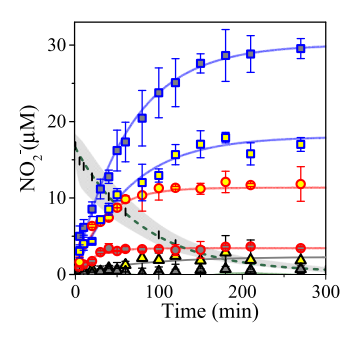


Figure 5. Nitrite formation at pH 1 in both nighttime (gray-filled symbols) and daytime (yellow-filled symbols) conditions. Green dashed line corresponds to the nitrite photolytic decay at pH 1 in the absence of the FA suspension.

increases, reaching a pseudo-steady-state concentration about 5 times and 2 times higher for USFA and INFA, respectively. Nevertheless, $\mathrm{NO_2}^-$ continues to be higher in EUFA than in any other sample examined here. This photolytic formation of $\mathrm{NO_2}^-$ suggests that the combustion process that generates FA plays a significant role in the formation pathways of nitrite during daytime.

As mentioned above, the thoroughly oxidized USFA and INFA result in an increased fraction of semiconductor metal oxide $\alpha\text{-Fe}_2\text{O}_3$ (with TiO_2 in smaller trace amounts) in the composition of the FA samples. The electron—hole pair generated by this rather small fraction of semiconductor metal oxide is enough to trigger a multiphase reaction that reduces NO_3^- , resulting in an indirect heterogeneous source of $\text{NO}_2^{-34,35,73,74}$

$$NO_3^-(a) + H_2O(a) + e_{cb}^- \rightarrow NO_2^-(a) + 2OH^-(a)$$
(14)

Furthermore, the oxidizing h_{vb}^+ can also react with nitrates near the surface to produce the nitrate radical, NO_3 , which readily photolyzes to form $NO_2^-(a)$, with the concomitant increase of NO_2^- in solution. ^{34,35} As mentioned above, a small fraction of NO_2^- formed in the reactions summarized in Schemes 1 and 2 under acidic conditions can form nitrous acid and partition into the gas phase

$$NO_2^-(aq) + H^+(aq) \rightleftharpoons HONO(aq) \rightleftharpoons HONO(g)$$
 (15)

In the case of thoroughly combusted samples, such as USFA and INFA, reactions 14 and 15 can provide a previously unrecognized pathway for daytime HONO formation. Scheme 2 represents the daytime competing mechanisms leading to iron mobility for both HCl and HNO₃ suspensions.

CONCLUSIONS AND ATMOSPHERIC IMPLICATIONS

Recent field and modeling studies suggest that reactions of iron on particles from combustion sources are significantly larger and more complex than previously estimated, with important implications in climate and Earth systems.¹⁷ In order to better understand the mechanisms involving iron dissolution from anthropogenic combustion particles, we carried out a comparative dissolution of FA from several coal-fired sources in two different acid media, HCl and HNO₃, at pHs 1.0 and 2.0, under anaerobic conditions. The effect of solar radiation on the iron dissolution pathways was also investigated, as it pertains to its role in iron mobility and speciation. In order to make the relevant comparisons of the samples, we normalized

Scheme 2. Iron Mobility from FA at Daytime, with $\equiv Fe^{2+}(s)$ Representing the Fe^{2+} Content within the Aluminosilicate of FA; Effect of Cu is Only Significant in EUFA Samples, where the Cu Content is Significantly Higher

$$= Fe^{2^{+}}_{(s)} \xrightarrow{\text{FeO}_{(s)}} \xrightarrow{\text{hv}} Fe^{2^{+}}_{(aq)} \xrightarrow{\text{e}^{-}_{cb}} Cu^{+}_{(aq)}$$

$$= Fe^{2^{+}}_{(s)}, FeO_{(s)} \xrightarrow{\text{Fe}_{2}O_{3(s)}} \xrightarrow{\text{hv}} Fe^{3^{+}}_{(aq)} \xrightarrow{\text{Fe}^{3^{+}}_{(aq)}} Cu^{2^{+}}_{(aq)}$$

$$= Fe^{2^{+}}_{(s)}, FeO_{(s)} \xrightarrow{\text{Hv}} Fe^{3^{+}}_{(aq)} \xrightarrow{\text{Fe}^{3^{+}}_{(aq)}} Cu^{2^{+}}_{(aq)}$$

$$= Fe^{2^{+}}_{(aq)} \xrightarrow{\text{Hv}} Fe^{3^{+}}_{(aq)} \xrightarrow{\text{hv}} Fe^{3^{+}}_{(aq)} + NO_{x}$$

$$= Fe^{2^{+}}_{(s)}, FeO_{(s)} \xrightarrow{\text{Hv}} Fe^{3^{+}}_{(aq)} \xrightarrow{\text{hv}} Fe^{3^{+}}_{(aq)} + NO_{x}$$

$$= Fe^{2^{+}}_{(s)}, FeO_{(s)} \xrightarrow{\text{Hv}} Fe^{3^{+}}_{(aq)} \xrightarrow{\text{hv}} Fe^{3^{+}}_{(aq)} \xrightarrow{\text{hv}} Fe^{3^{+}}_{(aq)} + NO_{x}$$

$$= Fe^{2^{+}}_{(s)}, FeO_{(s)} \xrightarrow{\text{Hv}} Fe^{3^{+}}_{(aq)} \xrightarrow{\text{hv}} Fe^{3^{+}}_{(aq)} \xrightarrow{\text{hv}} Fe^{3^{+}}_{(aq)} + NO_{x}$$

all quantified iron species to the total iron content in the samples, as determined by AAS analysis.

Several studies have suggested that mineralogy of ironcontaining aerosols and combustion particles plays a key role in iron solubility under atmospherically relevant conditions. ^{23,32,75,76} This mineralogy is driven by the fuel, source, and combustion efficiency. To date, FA studies have explored variation in the fuel^{20,23} or simply treat the combustion particles within a generalized category, implying no distinction based on the source region and combustion process.⁴ The data presented herein show that the acidic iron solubility depends greatly on the source region and combustion efficiency of the coal-fired power plants. These variables control the iron mineralogy of FA. Ultimately, our results clearly indicate that iron dissolution from FA is fundamentally controlled by two parameters: the composition of the combustion particles and the anion of the acid. The speciation of dissolved iron from FA samples is primarily controlled by the combustion efficiency. Our results indicate that dissolution of Fe²⁺ takes place from partially combusted samples, while more than 80% of the iron dissolved in thoroughly combusted samples was Fe³⁺. Incomplete combustion can also lead to reduced species in FA samples, which can open additional redox mechanisms affecting the speciation. Partial combustion processes can lead to larger particulate byproducts for some anthropogenic combustion processes, increasing the likelihood of particulate emissions. In fact, particulate emission decreases proportional to oxygen partial pressure or amount of oxygenated compounds during anthropogenic combustion processes. 77-79 No correlation was found between surface area and iron dissolution, suggesting that mineralogy and acid media are controlling the reaction over the surface contact interface.

The acidic media plays a fundamental role in the iron mobility from FA. Similar to mineral dust experiments reported in the literature, proton-promoted mechanisms observed in HCl suspensions are shown to be more efficient than the ligand-promoted mechanism in HNO₃ suspensions. Iron dissolution in the presence of sunlight was also explored and showed photoreduction pathways in HCl that, for the samples with the largest concentration of iron, mimic the photochemistry of mineral dust aerosols. 12,32,80 While nitric acid is less efficient dissolving the iron-containing particles, the surface-mediated reduction of nitrates into nitrites by Fe²⁺ contained in the particle resulted in mobility of only Fe³⁺. This nitrite formation appears to be a possible alternative pathway for the formation of atmospheric nitrous acid. In the presence of broadband light, at spectral regions where nitrites

photodegrade, the fully combusted FA particles lead to an increase in nitrite formation as a result of a larger fraction of semiconductor metal oxides in a mechanism that enhances the formation of nitrates.

ASSOCIATED CONTENT

Solution Supporting Information

The Supporting Information is available free of charge at https://pubs.acs.org/doi/10.1021/acsearthspace-chem.0c00057.

X-ray fluorescence spectral analysis of fly ash samples, infrared spectra of fly ash samples, X-ray fluorescence spectroscopy (XRF) elemental estimated percentage of trace elements in fly ash samples, atomic absorbance spectroscopy (AAS) analysis of iron and copper in fly ash samples, fraction of Fe species dissolved from fly ash, comparison of mass of Fe per surface area basis from fly ash at pH = 2.0, nitrite formation at pH 2 under dark conditions, and solution-phase copper in EUFA suspensions (pH 1.0) (pDF)

AUTHOR INFORMATION

Corresponding Author

Juan G. Navea — Chemistry Department, Skidmore College, Saratoga Springs, New York 12866-1632, United States; orcid.org/0000-0002-7723-6033; Email: jnavea@skidmore.edu

Authors

Deborah Kim – Chemistry Department, Skidmore College, Saratoga Springs, New York 12866-1632, United States

Yao Xiao – Chemistry Department, Skidmore College, Saratoga Springs, New York 12866-1632, United States

Renee Karchere-Sun — Chemistry Department, Skidmore College, Saratoga Springs, New York 12866-1632, United States

Emily Richmond – Chemistry Department, Skidmore College, Saratoga Springs, New York 12866-1632, United States

Heather M. Ricker – Chemistry Department, Skidmore College, Saratoga Springs, New York 12866-1632, United States

Angelina Leonardi – Chemistry Department, Skidmore College, Saratoga Springs, New York 12866-1632, United States

Complete contact information is available at: https://pubs.acs.org/10.1021/acsearthspacechem.0c00057

Notes

The authors declare no competing financial interest.

ACKNOWLEDGMENTS

This work was supported by NSF through the NSF Center for Aerosol Impacts on Chemistry of the Environment (CAICE), CHE-1801971.

REFERENCES

- (1) Elsner, M.; Schwarzenbach, R. P.; Haderlein, S. B. Reactivity of Fe(II)-bearing minerals toward reductive transformation of organic contaminants. *Environ. Sci. Technol.* **2004**, *38*, 799–807.
- (2) Falkowski, P. G.; Barber, R. T.; Smetacek, V. Biogeochemical controls and feedbacks on ocean primary production. *Science* **1998**, 281, 200–206.
- (3) Morel, F. M. M.; Price, N. M. The biogeochemical cycles of trace metals in the oceans. *Science* **2003**, *300*, 944–947.
- (4) Mahowald, N. M.; et al. Atmospheric iron deposition: Global distribution, variability, and human perturbations. *Annu. Rev. Mar. Sci.* **2009**, *1*, 245–278.
- (5) de Baar, H. J. W.; Boyd, P. M. The Role of Iron in Plankton Ecology and Carbon Dioxide Transfer of the Global Oceans. In *The Dynamic Ocean Carbon Cycle: A Midterm Synthesis of the Joint Global Ocean Flux Study*; Hanson, R. B., Ducklow, H. W., Field, J. G., Eds.; Cambridge University Press: Cambridge, 1999; pp 61–140.
- (6) Duce, R. A.; Tindale, N. W. Atmospheric transport of iron and its deposition in the ocean. *Limnol. Oceanogr.* **1991**, *36*, 1715–1726.
- (7) Fung, I. Y.; Meyn, S. K.; Tegen, I.; Doney, S. C.; John, J. G.; Bishop, J. K. B. Iron supply and demand in the upper ocean. *Global Biogeochem. Cycles* **1999**, *14*, 281–295.
- (8) Usher, C. R.; Michel, A. E.; Grassian, V. H. Reactions on mineral dust. *Chem. Rev.* **2003**, *103*, 4883–4940.
- (9) Rose, A. L.; Waite, T. D. Kinetic model for Fe(II) oxidation in seawater in the absence and presence of natural organic matter. *Environ. Sci. Technol.* **2002**, *36*, 433–444.
- (10) Hettiarachchi, E.; Hurab, O.; Rubasinghege, G. Atmospheric processing and iron mobilization of ilmenite: Iron-containing ternary oxide in mineral dust aerosol. *J. Phys. Chem. A* **2018**, *122*, 1291–1302.
- (11) Moore, J. K.; Doney, S. C.; Glover, D. M.; Fung, I. Y. Iron cycling and nutrient-limitation patterns in surface waters of the world ocean. *Deep Sea Res., Part II* 2001, 49, 463.
- (12) Fu, H.; Cwiertny, D. M.; Carmichael, G. R.; Scherer, M. M.; Grassian, V. H. Photoreductive dissolution of Fe-containing mineral dust particles in acidic media. *J. Geophys. Res.: Atmos.* **2010**, *115*, D11304.
- (13) Cwiertny, D. M.; Baltrusaitis, J.; Hunter, G. J.; Laskin, A.; Scherer, M. M.; Grassian, V. H. Characterization and acid-mobilization study of iron-containing mineral dust source materials. *J. Geophys. Res.* **2008**, *113*, D05202.
- (14) Cwiertny, D. M.; Young, M. A.; Grassian, V. H. Chemistry and photochemistry of mineral dust aerosol. *Annu. Rev. Phys. Chem.* **2008**, 59, 27–51.
- (15) Al-Abadleh, H. A. Review of the bulk and surface chemistry of iron in atmospherically relevant systems containing humic-like substances. *RSC Adv.* **2015**, *S*, 45785–45811.
- (16) Oakes, M.; Rastogi, N.; Majestic, B. J.; Shafer, M.; Schauer, J. J.; Edgerton, E. S.; Weber, R. J. Characterization of soluble iron in urban aerosols using near-real time data. *J. Geophys. Res.* **2010**, *115*, D15302.
- (17) Matsui, H.; Mahowald, N. M.; Moteki, N. et al. Anthropogenic combustion iron as a complex climate forcer. *Nat. Commun.* **2018**, 9 (). DOI: DOI: 10.1038/s41467-018-03997-0.
- (18) Borgatta, J.; Paskavitz, A.; Kim, D.; Navea, J. G. Comparative evaluation of iron leach from fly ash from different source regions under atmospherically relevant conditions. *Environ. Chem.* **2016**, *13*, 902–912.
- (19) Borgatta, J.; Navea, J. G. Fate of aqueous iron leached from tropospheric aerosols during atmospheric acidic processing: Study of

- the effect of humic-like substances. WIT Trans. Ecol. Environ. 2015, 198, 155.
- (20) Chen, H.; Laskin, A.; Baltrusaitis, J.; Gorski, C. A.; Scherer, M. M.; Grassian, V. H. Coal fly ash as a source of iron in atmospheric dust. *Environ. Sci. Technol.* **2012**, *46*, 2112–2120.
- (21) Ault, A. P.; Peters, T. M.; Sawvel, E. J.; Casuccio, G. S.; Willis, R. D.; Norris, G. A.; Grassian, V. H. Single-particle SEM-EDX analysis of iron-containing coarse particulate matter in an urban environment: Sources and distribution of iron within Cleveland, Ohio. *Environ. Sci. Technol.* **2012**, *46*, 4331–4339.
- (22) Chen, H.; Grassian, V. H. Iron dissolution of dust source materials during simulated acidic processing: The effect of sulfuric, acetic, and oxalic acids. *Environ. Sci. Technol.* **2013**, *47*, 10312–10321.
- (23) Fu, H.; Lin, J.; Shang, G.; Dong, W.; Grassian, V. H.; Carmichael, G. R.; Li, Y.; Chen, J. Solubility of iron from combustion source particles in acidic media linked to iron speciation. *Environ. Sci. Technol.* **2012**, *46*, 11119–11127.
- (24) 2013 Coal Combustion Product (CCP) Production & Use Survey Report; American Coal Ash Association: Aurora, CO, 2014.
- (25) Haque, M. E. Indian fly-ash: Production and consumption scenario. *Int. J. Waste Resour.* **2013**, *3*, 22.
- (26) Cai, X. P.; Zhang, S. Q.; Li, J. G. Research on treatment of zinc containing wastewater with fly ash zeolite. *Proceedings of the 2015 International Conference on Water Resources and Environment*; CRC Press, 2015; pp 35–37.
- (27) Feuerborn, H. Coal combustion products in Europe an update on production and utilisation standardization and regulation. *World of Coal Ash (WOCA) Conference*, 2011.
- (28) Navea, J. G.; Richmond, E.; Stortini, T.; Greenspan, J. Water adsorption isotherms on fly ash from several sources. *Langmuir* **2017**, 33, 10161–10171.
- (29) Losey, D. J.; Sihvonen, S. K.; Veghte, D. P.; Chong, E.; Freedman, M. A. Acidic processing of fly ash: Chemical characterization, morphology, and immersion freezing. *Environ. Sci.: Processes Impacts* **2018**, 20, 1581–1592.
- (30) Freedman, M. A.; Ott, E.-J. E.; Marak, K. E. Role of pH in aerosol processes and measurement challenges. *J. Phys. Chem. A* **2019**, 123, 1275–1284.
- (31) Hettiarachchi, E.; Reynolds, R. L.; Goldstein, H. L.; Moskowitz, B.; Rubasinghege, G. Bioavailable iron production in airborne mineral dust: Controls by chemical composition and solar flux. *Atmos. Environ.* **2019**, 205, 90.
- (32) Hettiarachchi, E.; Rubasinghege, G. Mechanistic study on iron solubility in atmospheric mineral dust aerosol: Roles of titanium, dissolved oxygen, and solar flux in solutions containing different acid anions. ACS Earth Space Chem. 2019, 4, 101–111.
- (33) Navea, J. G.; Grassian, V. H. Photochemistry of atmospheric particles. Reference Module in Chemistry, Molecular Sciences and Chemical Engineering; Elsevier, 2017.
- (34) Lesko, D. M. B.; Coddens, E. M.; Swomley, H. D.; Welch, R. M.; Borgatta, J.; Navea, J. G. Photochemistry of nitrate chemisorbed on various metal oxide surfaces. *Phys. Chem. Chem. Phys.* **2015**, *17*, 20775–20785.
- (35) Ostaszewski, C. J.; Stuart, N. M.; Lesko, D. M. B.; Kim, D.; Lueckheide, M. J.; Navea, J. G. Effects of coadsorbed water on the heterogeneous photochemistry of nitrates adsorbed on TiO₂. *J. Phys. Chem. A* **2018**, *122*, 6360–6371.
- (36) Chen, H.; Navea, J. G.; Young, M. A.; Grassian, V. H. Heterogeneous photochemistry of trace atmospheric gases with components of mineral dust aerosol. *J. Phys. Chem. A* **2011**, *115*, 490–499.
- (37) Hwang, C.-L.; Chiang, C.-H.; Huynh, T.-P.; Vo, D.-H.; Jhang, B.-J.; Ngo, S.-H. Properties of alkali-activated controlled low-strength material produced with waste water treatment sludge, fly ash, and slag. *Constr. Build. Mater.* **2017**, *135*, 459.
- (38) Wang, M.; Zhao, H.; Liu, Y.; Kong, C.; Yang, A.; Li, J. Removal of Fe from fly ash by carbon thermal reduction. *Microporous Mesoporous Mater.* **2017**, 245, 133.

- (39) Bargar, J. R.; Kubicki, J. D.; Reitmeyer, R.; Davis, J. A. ATR-FTIR spectroscopic characterization of coexisting carbonate surface complexes on hematite. *Geochim. Cosmochim. Acta* **2005**, *69*, 1527.
- (40) White, S. C.; Case, E. D. Characterization of fly ash from coal-fired power plants. *J. Mater. Sci.* **1990**, 25, 5215–5219.
- (41) Srinivasachar, S.; Helble, J. J.; Boni, A. A. Mineral behavior during coal combustion 1. pyrite transformations. *Prog. Energy Combust. Sci.* **1990**, *16*, 281.
- (42) Li, W.; Shao, L. Transmission electron microscopy study of aerosol particles from the brown hazes in northern China. *J. Geophys. Res.* **2009**, *114*, D09302.
- (43) Mueller, S. F.; Mallard, J. W.; Mao, Q.; Shaw, S. L. Fugitive particulate emission factors for dry fly ash disposal. *J. Air Waste Manage. Assoc.* **2013**, *63*, 806.
- (44) Vukić, J.; Fott, J.; Petrusek, A.; Šanda, R. What can size distribution of spheroidal carbonaceous particles reveal about their source? *Atmos. Environ.* **2006**, *40*, 3527–3535.
- (45) Umo, N. S.; Murray, B. J.; Baeza-Romero, M. T.; et al. Ice nucleation by combustion ash particles at conditions relevant to mixed-phase clouds. *Atmos. Chem. Phys.* **2015**, *15*, 5195–5210.
- (46) Roca, M.; Zahardis, J.; Bone, J.; El-Maazawi, M.; Grassian, V. H. 310 nm irradiation of atmospherically relevant concentrated aqueous nitrate solutions: Nitrite production and quantum yields. *J. Phys. Chem. A* 2008, *112*, 13275–13281.
- (47) Rubasinghege, G.; Lentz, R. W.; Scherer, M. M.; Grassian, V. H. Simulated atmospheric processing of iron oxyhydroxide minerals at low pH: Roles of particle size and acid anion in iron dissolution. *Proc. Natl. Acad. Sci. U.S.A.* **2010**, *107*, 6628–6633.
- (48) Zinder, B.; Furrer, G.; Stumm, W. The coordination chemistry of weathering: II. dissolution of Fe(III) oxides. *Geochim. Cosmochim. Acta* **1986**, *50*, 1861–1869.
- (49) Sulzberger, B.; Suter, D.; Siffert, C.; Banwart, S.; Stumm, W. Dissolution of Fe(III)(hydr)oxides in natural waters; laboratory assessment on the kinetics controlled by surface coordination. *Mar. Chem.* **1989**, 28, 127–144.
- (50) Remucal, C. K.; Sedlak, D. L. The role of iron coordination in the production of reactive oxidants from ferrous iron oxidation by oxygen and hydrogen peroxide. *Aquatic Redox Chemistry*; American Chemical Society, 2011; Vol 1071, pp 177–197.
- (51) Winburn, R. S.; Grier, D. G.; McCarthy, G. J.; Peterson, R. B. Rietveld quantitative X-ray diffraction analysis of NIST fly ash standard reference materials. *Powder Diffr.* **2000**, *15*, 163–172.
- (52) Gieré, R.; Blackford, M.; Smith, K. TEM Study of PM2.5Emitted from Coal and Tire Combustion in a Thermal Power Station. *Environ. Sci. Technol.* **2006**, *40*, 6235–6240.
- (53) Tomeczek, J.; Palugniok, H. Kinetics of mineral matter transformation during coal combustion1. Fuel 2002, 81, 1251.
- (54) Baker, A. R.; Jickells, T. D. Mineral particle size as a control on aerosol iron solubility. *Geophys. Res. Lett.* **2006**, 33 (). doi: DOI: 10.1029/2006GL026557.
- (55) Brombacher, C.; Bachofen, R.; Brandl, H. Development of a Laboratory-Scale Leaching Plant for Metal Extraction from Fly Ash by ThiobacillusStrains. *Appl. Environ. Microbiol.* **1998**, *64*, 1237–1241.
- (56) Wu, P.; Tang, Y.; Cai, Z. Dual role of coal fly ash in copper ion adsorption followed by thermal stabilization in a spinel solid solution. *RSC Adv.* **2018**, *8*, 8805–8812.
- (57) Mao, J.; Fan, S.; Jacob, D. J.; Travis, K. R. Radical loss in the atmosphere from Cu-Fe redox coupling in aerosols. *Atmos. Chem. Phys.* **2013**, *13*, 509–519.
- (58) Mao, J.; Fan, S.; Horowitz, L. W. Soluble Fe in aerosols sustained by gaseous HO₂ uptake. *Environ. Sci. Technol. Lett.* **2017**, *4*, 98–104.
- (59) Deguillaume, L.; Leriche, M.; Desboeufs, K.; Mailhot, G.; George, C.; Chaumerliac, N. Transition Metals in Atmospheric Liquid Phases. Sources, Reactivity, and Sensitive Parameters. *Chem. Rev.* **2005**, *105*, 3388–3431.
- (60) Baltrusaitis, J.; Schuttlefield, J.; Jensen, J. H.; Grassian, V. H. FTIR spectroscopy combined with quantum chemical calculations to investigate adsorbed nitrate on aluminium oxide surfaces in the

- presence and absence of co-adsorbed water. *Phys. Chem. Chem. Phys.* **2007**, *9*, 4970–4980.
- (61) Bard, A. J.; Parsons, R.; Jordan, J. Standard Potentials in Aqueous Solution; Routledge: New York, 1985.
- (62) Hofstetter, T. B.; Schwarzenbach, R. P.; Haderlein, S. B. Reactivity of Fe(II) species associated with clay minerals. *Environ. Sci. Technol.* **2003**, *37*, 519–528.
- (63) Hofstetter, T. B.; Neumann, A.; Schwarzenbach, R. P. Reduction of nitroaromatic compounds by Fe(II) species associated with iron-rich smectites. *Environ. Sci. Technol.* **2006**, *40*, 235–242.
- (64) Zhu, X.; Prospero, J. M.; Savoie, D. L.; Millero, F. J.; Zika, R. G.; Saltzman, E. S. Photoreduction of iron(III) in marine mineral aerosol solutions. *J. Geophys. Res.* **1993**, *98*, 9039–9046.
- (65) Devi, L. G.; Munikrishnappa, C.; Nagaraj, B.; Rajashekhar, K. E. Effect of chloride and sulfate ions on the advanced photo fenton and modified photo fenton degradation process of alizarin red S. J. Mol. Catal. A: Chem. 2013, 374–375, 125–131.
- (66) Brüggemann, M.; Hayeck, N.; George, C. Interfacial photochemistry at the ocean surface is a global source of organic vapors and aerosols. *Nat. Commun.* **2018**, *9*, 2101.
- (67) Zafiriou, O. C.; True, M. B. Nitrite photolysis as a source of free radicals in productive surface waters. *Geophys. Res. Lett.* **1979**, *6*, 81–84.
- (68) Goldstein, S.; Rabani, J. Mechanism of nitrite formation by nitrate photolysis in aqueous solutions: the role of peroxynitrite, nitrogen dioxide, and hydroxyl radical. *J. Am. Chem. Soc.* **2007**, *129*, 10597–10601.
- (69) Benedict, K. B.; McFall, A. S.; Anastasio, C. Quantum yield of nitrite from the photolysis of aqueous nitrate above 300 nm. *Environ. Sci. Technol.* **2017**, *51*, 4387–4395.
- (70) Burkholder, J. B.; Abbatt, J. P. D.; Barnes, I.; et al. The essential role for laboratory studies in atmospheric chemistry. *Environ. Sci. Technol.* **2017**, *51*, 2519–2528.
- (71) Ng, N. L.; Brown, S. S.; Archibald, A. T.; et al. Nitrate radicals and biogenic volatile organic compounds: Oxidation, mechanisms, and organic aerosol. *Atmos. Chem. Phys.* **2017**, *17*, 2103–2162.
- (72) Silveira, J. E.; Paz, W. S.; Garcia-Muñoz, P.; Zazo, J. A.; Casas, J. A. UV-LED/ilmenite/persulfate for azo dye mineralization: The role of sulfate in the catalyst deactivation. *Appl. Catal., B* **2017**, 219, 314—321
- (73) Nanayakkara, C. E.; Jayaweera, P. M.; Rubasinghege, G.; Baltrusaitis, J.; Grassian, V. H. Surface photochemistry of adsorbed nitrate: The role of adsorbed water in the formation of reduced nitrogen species on α -Fe₂O₃ particle surfaces. *J. Phys. Chem. A* **2014**, 118, 158–166.
- (74) Schuttlefield, J.; Rubasinghege, G.; El-Maazawi, M.; Bone, J.; Grassian, V. H. Photochemistry of adsorbed nitrate. *J. Am. Chem. Soc.* **2008**, *130*, 12210–12211.
- (75) Schroth, A. W.; Crusius, J.; Sholkovitz, E. R.; Bostick, B. C. Iron solubility driven by speciation in dust sources to the ocean. *Nat. Geosci.* **2009**, *2*, 337–340.
- (76) Majestic, B. J.; Schauer, J. J.; Shafer, M. M. Application of synchrotron radiation for measurement of iron red-ox speciation in atmospherically processed aerosols. *Atmos. Chem. Phys.* **2007**, *7*, 2475–2487.
- (77) Patiño, P.; Méndez, M.; Pastrán, J.; Gambús, G.; Navea, J.; Escobar, O.; Castro, A. Oxidation of Cycloalkanes and Diesel Fuels by Means of Oxygen Low Pressure Plasmas. *Energy Fuels* **2002**, *16*, 1470–1475.
- (78) Gambús, G.; Patiño, P.; Navea, J. Spectroscopic study of low-pressure water plasmas and their reactions with liquid hydrocarbons. *Energy Fuels* **2002**, *16*, 172–176.
- (79) Gambús, G.; Patiño, P.; Méndez, B.; Sifontes, A.; Navea, J.; Martín, P.; Taylor, P. Oxidation of long chain hydrocarbons by means of low-pressure plasmas. *Energy Fuels* **2001**, *15*, 881–886.
- (80) Faust, B. C.; Hoffmann, M. R. Photoinduced reductive dissolution of α -iron oxide (α -Fe₂O₃) by bisulfite. *Environ. Sci. Technol.* **1986**, 20, 943–948.